

INTERACTION OF ATOMIC OXYGEN WITH A POLYCRYSTALLINE Au SURFACE: XPS AND TPD STUDY

A. I. Stadnichenko^{1*}, S. V. Koshcheev¹,
and A. I. Boronin¹

Adsorption of atomic oxygen on the surface of polycrystalline gold is studied in detail by XPS and TPD methods. It is shown that the action of atomic oxygen at initial stages leads to the formation of chemisorbed atomic oxygen with the deposition thickness $\Theta = 0-0.5$ monolayers. Increased exposure to atomic oxygen leads to the formation of 2D gold oxide. At the maximum oxygen saturation, the calculated oxide layer thickness is 3 Å, and its stoichiometry is close to AuO₂. The TPD analysis shows that thermal stability of adsorbed oxygen is 510 K for the chemisorbed layer and 525 K for the 2D gold oxide. The structure of the 2D gold oxide is determined as one layer of gold atoms and two layers of oxygen atoms adsorbed on the surface and inside the subsurface layer. The reactivity of adsorbed oxygen is tested by the interaction of CO and H₂ at room temperature; all the oxygen forms are shown to be active. It is established that the reactivity towards CO is 2 orders of magnitude higher than towards H₂, suggesting that oxygen species take part in the PROX mechanism.

DOI: 10.1134/S0022476623050062

Keywords: gold oxide, atomic oxygen, surface, CO oxidation, XPS, TPD.

INTRODUCTION

The interest in the use of gold catalysts was initiated by the research by Haruta [1, 2] and has significantly increased over the past 20 years [3-12]. Gold-based catalysts are highly active in many processes, particularly in reactions of complete [3, 7, 8, 13, 14], selective [15-19], and partial [3, 20, 21] oxidation. To date, the following most important aspects affecting catalytic activity of gold have been identified: particle size, nature and morphology of the support, synthesis methods, activation treatment, etc. In the field of treatment, numerous works have already been published, and their number is rapidly increasing. The mechanism of oxidation is largely determined by oxygen species, so their nature is essential for the understanding of reaction mechanisms.

For many metals employed in catalysis, fundamental studies of oxygen forms on model systems such as single crystals, foils, and thin films were carried out many years ago [22-24]. But the states of oxygen on the surface of gold and the activity of the latter have not been precisely established, since gold is commonly considered nonreactive in catalytic processes [7, 25]. The study of gold oxidation is also complicated by the need of using oxygen activation. There are several ways of gold oxidation: gas-phase microwave or high-frequency discharge [26-28], low-temperature UV- and electron-

¹Boreskov Institute of Catalysis, Siberian Branch, Russian Academy of Sciences, Novosibirsk, Russia; *stad@catalysis.ru. Original article submitted March 1, 2023; revised March 22, 2023; accepted March 27, 2023.

induced oxygen adsorption [29, 30], application of atomic oxygen [31-35], oxygen ion sputtering [36]; oxidation by aggressive gases (e.g. ozone) [37-40], magnetron sputtering [41, 42], pulsed laser sputtering in O₂ [43]; electrochemical oxidation of gold surfaces in acids [44, 45]. All these methods are relatively laborious and lead to different degrees of gold oxidation.

Weakly charged metallic [46-48] gold in δ^+ [6, 49] and δ^- [50] states or 1+/3+ oxidized gold forms [51] are commonly considered as reactive oxygen species. At present, conducting a systematic study of oxygen species on the surface of gold, especially at the early stages of gold oxidation, is an urgent task. The main goal of our work is to study initial stages of gold surface oxidation by flowing atomic oxygen. This method combines the efficiency of gold oxidation, the softness of surface treatment, and good reproducibility of treatment conditions.

EXPERIMENTAL

X-ray photoelectron spectroscopy. The experiments were carried out on a VG ESCALAB HP X-ray photoelectron spectrometer equipped with analyzer and preparation chambers. After placing a sample in the analyzer chamber, the spectra were recorded using the AlK α non-monochromatic X-ray radiation ($h\nu = 1486.6$ eV). The source power was 200 W in all experiments. The diameter of the X-ray beam was ~ 8 mm. The charge states of gold and oxygen forms in the resulting AuO_x oxide layers were studied by recording narrow spectral regions O 1s and Au 4f with a step of 0.1 eV. Surface contamination was controlled by recording high-sensitivity survey spectra. Data processing and spectral analysis (curve fitting, area calculation) were carried out by standard graphic programs and by the Calc-XPS program that was previously tested on a number of systems [52-55]. When performing component decomposition, the peaks were approximated by a sum of Lorentz and Gaussian functions while using background subtraction with the Shirley method. The error of background subtraction and component deconvolution did not exceed 2-3%.

The spectrometer was also equipped with a Q7B quadrupole mass spectrometer (Vacuum Generators) installed in the analyzer chamber close to the sample surface to provide a good signal/background ratio in the mass spectra. A total of 18, 32, 28, and 44 masses were simultaneously recorded in all the TPD experiments.

Sample preparation. The sample was a 0.2 mm thick polycrystalline gold foil (99.99% purity) with a size of 12×8 mm. The clean gold surface was prepared by multiple successive cycles of argon ion bombardment and subsequent annealing at 923 K in the preparation chamber. The sample was subjected to resistive heating. Its temperature was controlled using a platinum:platinum-rhodium thermocouple that was spot welded to the opposite side of the foil. The adsorbed oxygen species and AuO_x layers were prepared by treating a pure gold surface by a flow of partially atomized oxygen. Atomic oxygen was obtained in a gas flow ($P_{O_2} = 1 \cdot 10^{-7}$ mbar) using hot ($T \sim 1673$ K) platinum foil (20 μ m thick Pt foil, 4×15 mm, 99.99% purity). The oxidized surface was located perpendicular to a hot fiber at a distance of ~ 2 cm from the latter. Possible sputtering of the Pt atomizer was controlled by XPS by the absence of peaks in Pt 4f and Pt 4d spectral regions and by TPD by the absence of peaks in the O₂ mass spectrum due to the decomposition of platinum oxides with $T_{max} = 475$ K and 623 K. No Pt sputtering was observed in all the experimental cycles.

Stepwise reduction of the gold oxide surface was carried out at 298 K in the preparation chamber as a result of CO exposure with a total value from 10 to 100 langmuir (L). Dynamic reduction of the gold oxide surface was studied in the analyzer chamber in the dynamic XPS mode under a gas pressure (CO, C₂H₄ or H₂) of $4 \cdot 10^{-7}$ mbar at 373 K.

Quantitative computations. The amount of oxygen adsorbed on the gold surface was estimated by two different methods. The first one was based on the calculation of the adsorbate amount using the modified formula by Matloob and Roberts [56]. The second one was based on analyzing the decrease of the XPS signal of metallic gold (Au 4f_{7/2} = 84.0 eV) depending on the thickness of the screening oxidized gold layers [57]. Assuming homogeneous adsorbate distribution, the thickness of screening layers can be calculated independently on the composition of the screening layers as follows:

$$d = -\lambda \cdot \sin(\alpha) \cdot \ln(I / I_0),$$

where d is the thickness of the screening layer; λ is the free path length; I_0 is the XPS signal of pure gold; I is the XPS signal of metallic gold coated with an oxide film with thickness d registered for the electron beam angle α .

It was assumed that one monolayer consists of 10^{15} atoms per 1 cm^2 ; the free path length was taken equal to $\lambda = 20\text{ \AA}$ [58]. This value is the average of mean free paths of electrons through gold ($\lambda_{\text{Au}} = 15\text{ \AA}$) and oxygen ($\lambda_{\text{O}} = 36\text{ \AA}$) atoms constituting the shielding layer. Quantitative contents of elements were obtained by comparing the areas under the corresponding XPS lines while taking into account the ASF atomic sensitivity factors [59].

Reactivity computation. The reactivity was calculated as the ratio of the number of reactions between CO and oxygen molecules adsorbed on the gold surface to the total number of CO impacts on the sample surface. The series of O 1s and Au 4f spectra obtained by stepwise AuO_x reduction was processed to calculate the reactivity. The XPS data (O 1s and Au 4f spectra) were analyzed using deconvolution into spectral components to determine the amount of individual oxygen species. The procedure for computing the reaction probability was described in more detail in [53, 60].

Thermal stability. The TPD study of adsorbed oxygen layers was performed by combining the dynamic spectroscopy of the intensity of the O 1s core level ($E_b = 529.6\text{ eV}$, 5 s per point) and the mass-spectrometry registration of the O₂ partial pressure. The accuracy of dynamic XPS was improved by using increased analyzer transmission energy $HV = 100\text{ eV}$. The sample was heated from room temperature to 723 K at a heating rate of 2 K/s. To avoid possible changes in the dynamic XPS signal due to the motion or deformation of the sample during heating, all signals were normalized to the background line signal ($E_b = 495.0\text{ eV}$). Also, a set of O 1s and Au 4f spectra were obtained by stepwise heating with a step in of 40 K to determine the behavior of oxygen and gold forms upon heating. All the methods gave similar results.

RESULTS AND DISCUSSION

Fig. 1 shows the Au 4f and O 1s XPS spectra of gold surface depending on the time of exposure to atomic oxygen (0 min, 1 min, 5 min, 10 min, 15 min, 20 min, 55 min, 105 min, 160 min, respectively). As can be seen from Fig. 1a, the intensity of the Au 4f line decreases and unresolved peaks (shoulders) appear at high binding energies as the time of exposure to atomic oxygen increases. After the treatment, the binding energy (E_b) of the Au 4f_{7/2} peak remains close to $E_b \sim 84.0\text{ eV}$. This indicates that their electronic states of gold atoms in the analysis zone (less than 60 Å) did not change. The decrease of Au 4f line intensity may be caused by structural changes in the surface layers of gold and by the screening of bulk gold metal by a layer of adsorbed oxygen.

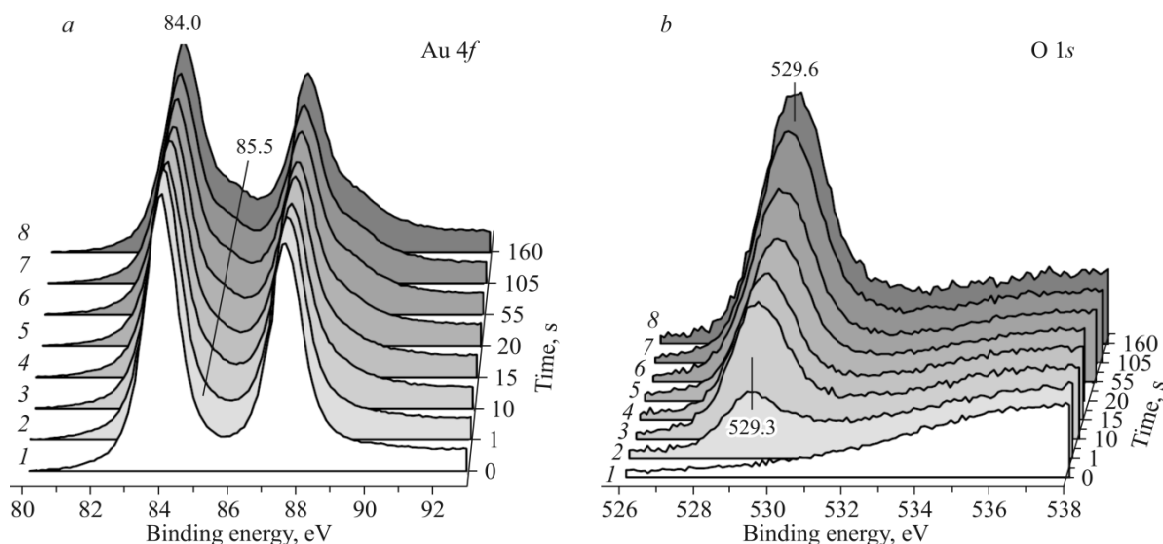


Fig. 1. Au 4f (a) and O 1s (b) XPS spectra of the gold surface exposed to atomic oxygen for 0 min (1), 1 min (2), 10 min (3), 15 min (4), 20 min (5), 55 min (6), 105 min (7), 160 min (7).

Fig. 1b shows the O 1s spectra for the surface treated with atomic oxygen, depending on the exposure time. Within the sensitivity of the XPS method, no oxygen species were found on the initially pure gold surface. After 1-5 min of exposure, an oxygen peak with $E_b(\text{O } 1s) = 529.3 \text{ eV}$ appeared in the XPS spectra. As the exposure time increased, the position of the O 1s peak gradually shifted towards higher binding energies up to 529.6 eV. After 50 min of exposure, no further changes in the O 1s spectra were observed. The full width at half maximum (FWHM) of the O 1s peak exceeded 2 eV. This value is much larger than the experimental resolution for the O 1s line (1.6 eV for the analyzer transmission energy $HV = 20$); therefore, the observed O 1s spectrum contains more than one component.

For the preliminary analysis of changes in the state of gold exposed to the influence of atomic oxygen, we obtained a series of difference spectra between the Au 4f line of the gold surface exposed to atomic oxygen and the Au 4f spectrum of the pure gold surface (Fig. 2a). Peaks with negative intensities in the difference spectra signify the disappearance of gold atoms with a given electronic and geometric configuration of the initial state of pure surface, while the peaks with positive intensities reflect the appearance of gold atoms or ions with new electronic and geometric configurations due to the chemical interaction with oxygen [57]. The difference spectra indicate with a sufficiently high accuracy of $\pm 0.2 \text{ eV}$ the presence of individual components in the integrated spectra corresponding to surface gold atoms, both bound to oxygen atoms and unbound ones.

At the initial interaction stages (Fig. 2a, 1), the intensity of the Au 4f peak with $E_b(\text{Au } 4f_{7/2}) = 83.6 \text{ eV}$ decreases, while that of the peak with $E_b = 84.6 \text{ eV}$ increases. With increasing exposure time (Fig. 2a, 2 and 3), the intensity of the Au 4f_{7/2} peak with $E_b = 84.0 \text{ eV}$ gradually decreased, while that of the peak with $E_b(\text{Au } 4f_{7/2}) = 85.6 \text{ eV}$ increased.

The electronic properties of the metal surface layer differ from those of the bulk metal and are manifested as a shift of the lines of the metal ground level on the binding energy scale [61, 62]. It is known for gold that the E_b shift of surface atoms relative to bulk atoms is negative ($\Delta E_b^{s/b} < 0$) [63]. Thus, the observed decrease of the intensity of the peak at $E_b(\text{Au } 4f_{7/2}) = 83.6 \text{ eV}$ can be explained by decreased number of low-coordinated metallic gold atoms directly on the surface. The observed intensity decrease at 84.0 eV corresponds to the decreased number of bulk gold atoms due to their oxidation in the subsurface region. The components with E_b higher than 84.0 eV correspond to the formation of oxidized gold atoms. Apparently, the forms of gold with $E_b(\text{Au } 4f_{7/2}) = 84.6 \text{ eV}$ are related to its oxidized atoms on the surface, since the ground level $\Delta E_{\text{cb}}^{s/b}(\text{ox}) = E_{\text{cb}}(\text{Au } 4f_{\text{surf}})_{\text{ox}} - E_b(\text{Au } 4f_{\text{surf}})_{\text{met}}$ is shifted by $\sim 1.0 \text{ eV}$ towards higher binding energies, thus indicating

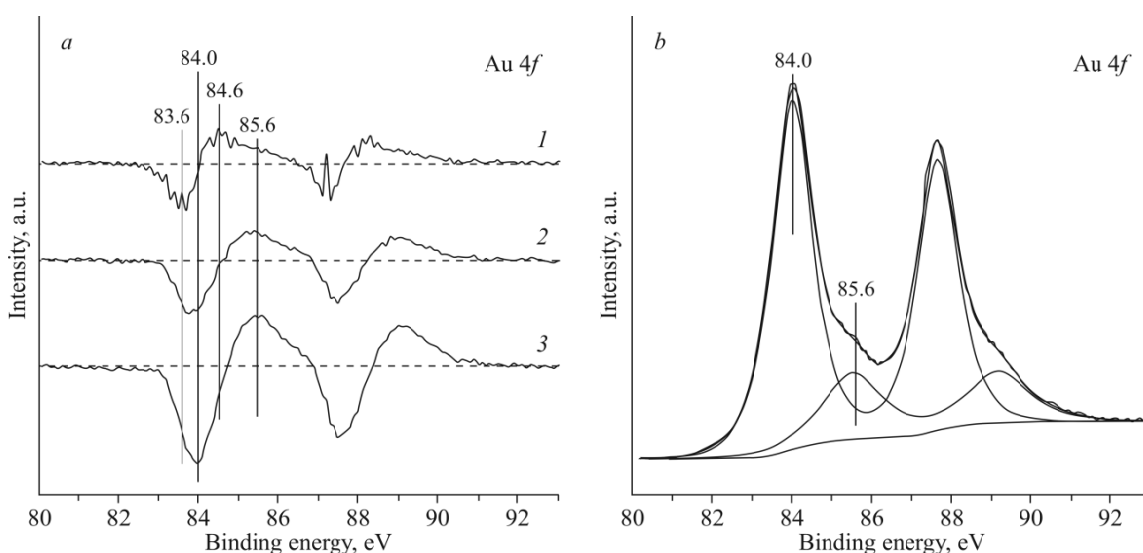


Fig. 2. Difference Au 4f spectra obtained by the subtraction of the Au 4f line of pure gold from the signal of gold surface exposed to atomic oxygen for 1 min (1), 10 min (2), and 55 min (3) (a); individual components of the deconvoluted Au 4f spectrum after 55 min of exposure to atomic oxygen (b).

the oxidation of surface low-coordinated atoms. The peak with $E_b(\text{Au } 4f_{7/2}) = 85.6 \text{ eV}$ can be assigned to the gold oxide structure in subsurface layers.

The above analysis of the difference Au 4*f* spectra revealed information on the formation of oxidized gold states under the influence of atomic oxygen. However, individual gold components corresponding to these surface particles could not be correctly identified by the deconvolution of Au 4*f* spectra into individual components. This may be due to two reasons. First, the surface of the polycrystalline foil contains a wide range of surface gold particles with different geometric and electronic properties. Thus, the contribution of these particles into the XPS spectrum is diffused by $\sim 84.6 \text{ eV}$. Second, the contribution of each surface state to the integral Au 4*f* spectrum is very small and cannot be unambiguously distinguished. The data obtained from the difference Au 4*f* spectra agree with the concept of diminished binding energies for surface gold atoms and a shift towards higher binding energies upon the transition from the metallic state to the oxidized one.

Reliable decomposition of the Au 4*f* spectrum was achieved for oxidized gold surfaces after prolonged exposure to atomic oxygen when the number of oxidized gold atoms was sufficiently large. Fig. 2*b* shows an example of such decomposition of the XPS spectrum registered after a 55 minute exposure to a flow of atomic oxygen. The Au 4*f* spectrum contains two doublets with Au 4*f*_{7/2} maxima at 84.0 eV and $\sim 85.5 \text{ eV}$ which can be assigned to metallic gold and to oxidized gold close to the Au(3+) state [28, 43, 46]. Note that the E_b value and the half-width of the Au 4*f* doublet describing the metallic state of gold were in all cases constant and equal to 84.0 eV and 1.2 eV, respectively. As the exposure time increased, the position of the Au(3+) oxidized gold component shifted towards higher binding energies (from 85.4 eV to 85.6 eV), which was accompanied by a gradual half-width decrease. This behavior indicates increased amount of oxygen on the surface and structural ordering of the oxide layer.

The deconvolution of O 1*s* spectra into individual components after the exposure to atomic oxygen revealed several forms of oxygen on the surface. Initially, the flow of atomic oxygen interacted with the gold surface to form an oxygen species characterized by a peak with $E_b(\text{O } 1s) = 529.3 \text{ eV}$ (Fig. 3*a*). Apparently, this state represents atomic oxygen chemisorbed on the gold surface without penetrating inside the volume. This binding energy is characteristic of oxygen species chemisorbed on various metals and has been reported by many authors in the studies of gold surface [32, 37]. Note that the O 1*s* spectrum shows other oxygen states with higher binding energies (530.7 eV, 531.8 eV, and 532.8 eV). The peaks at 531.8 eV and 532.8 eV have low intensities; therefore, it cannot be excluded that their appearance is due to trace amounts of carbon-oxygen containing particles on the surface [26]. The component with $E_b(\text{O } 1s) = 530.7 \text{ eV}$ can be assigned to the formation of –OH or peroxide and/or superoxide groups on the surface [64]. Note that oxygen with $E_b(\text{O } 1s) = 530.7 \text{ eV}$ was the main component observed on the surface of gold films prepared by laser ablation in oxygen [43]. Thus prepared gold samples contain numerous defects, and the observed oxygen species are apparently stabilized on the defective sides of the surface.

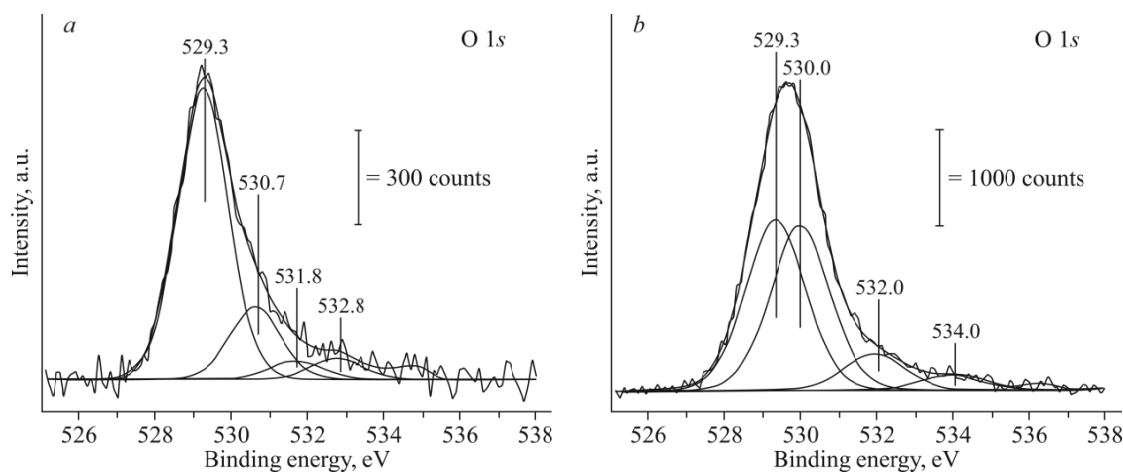


Fig. 3. Components of O 1*s* XPS spectra of the gold surface oxidized by atomic oxygen for 1 min (a), 160 min (b).

The decomposition of O 1s spectra obtained after prolonged exposure to atomic oxygen showed the formation of a new state with $E_b(\text{O } 1s) = 530.0 \text{ eV}$. The intensity of this peak increases with exposure time and is equal to that of the component at 529.3 eV for a 160 minute exposure (Fig. 3b). The E_b values of low-intensity oxygen peaks for the gold surface oxidized by a 160 minute exposure are quite high (532.0 eV and 534.0 eV) and cannot be interpreted as oxide forms or oxygen adsorbed on the metal surface. Apparently, these oxygen forms are the oxygen of adsorbed water and/or hydrocarbon impurities [26] or peroxide-like particles located on the oxide film defects.

The obtained XPS data were used to calculate the thickness of the oxidized layers and the Au/O ratio (Fig. 4). The oxygen coating calculated from the intensity of O 1s spectra increased with increasing exposure time to reach a maximum value of ~ 1.7 monolayer (ML) (Fig. 4, 1). The maximum number of oxidized gold atoms estimated from the Au 4f intensity was ~ 1.2 ML. This value was reached after a 55 minute exposure and then did not increase (Fig. 4, 2). Equal amounts of oxygen atoms and oxidized gold observed at the initial oxidation stages correspond to the adsorption of oxygen atoms on the surface with the Au:O = 1:1 stoichiometry. The shift of the integral peak O 1s towards higher binding energies was observed exactly after the exposure to atomic oxygen for 50 or more minutes. This effect was accompanied by the appearance of a peak at $E_b(\text{O } 1s) = 530.0 \text{ eV}$.

It can be assumed that adsorbed oxygen transforms into a 2D oxide structure at the initial oxidation stages. After reaching the critical concentration of surface oxygen atoms, they diffuse into the subsurface layer (determined here as the space between the first and second layers of gold atoms) to form a 2D oxide consisting of a single layer of oxygen atoms on the surface (α_1 - $E_b(\text{O } 1s) = 529.3 \text{ eV}$), one layer of oxidized gold atoms (β - $E_b(\text{Au } 4f) = 85.6 \text{ eV}$), and one layer of oxygen atoms below the layer of oxidized gold (α_2 - $E_b(\text{O } 1s) = 530.0 \text{ eV}$). The estimated stoichiometric composition of the most oxidized surface is $[\alpha_1]:[\beta]:[\alpha_2] = 0.96:1.0:1.17$ and it determines the stoichiometry of the 2D gold oxide AuO_2 . The thickness of the outer layer screening the metal (Fig. 4, 3) increased fast enough at the initial oxidation stages and almost did not change at the final stages when the amount of surface oxygen increased. It can be assumed that the adsorbed oxygen diffused into the structure of the resulting 2D oxide by filling oxygen vacancies. The estimated outer layer thickness (d) corresponds to that of the 2D oxide film ($\sim 3.2 \text{ \AA}$), which is quite a reasonable value within the proposed 2D oxide model.

Thermal stability of the obtained oxygen species was estimated using TPD experiments for adsorption layers with different oxygen coatings. Thermal desorption of chemisorbed oxygen obtained during a 1 minute exposure to atomic oxygen was observed at 510 K (Fig. 5a, 1). The peak in the TPD spectra showed a noticeable asymmetry: smooth increase before and sharp decline after the maximum. This form of desorption curves is typical for the phase decomposition with zero pumping

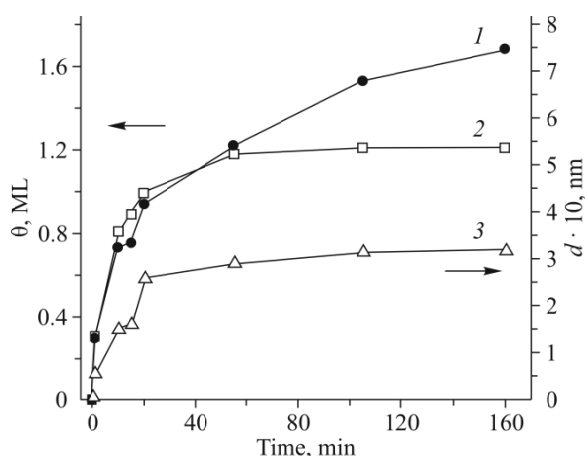


Fig. 4. Oxygen coating, monolayers (1); coating by oxidized gold atoms, monolayers (2), thickness of the oxidized gold layer as a function of exposure to atomic oxygen (3).

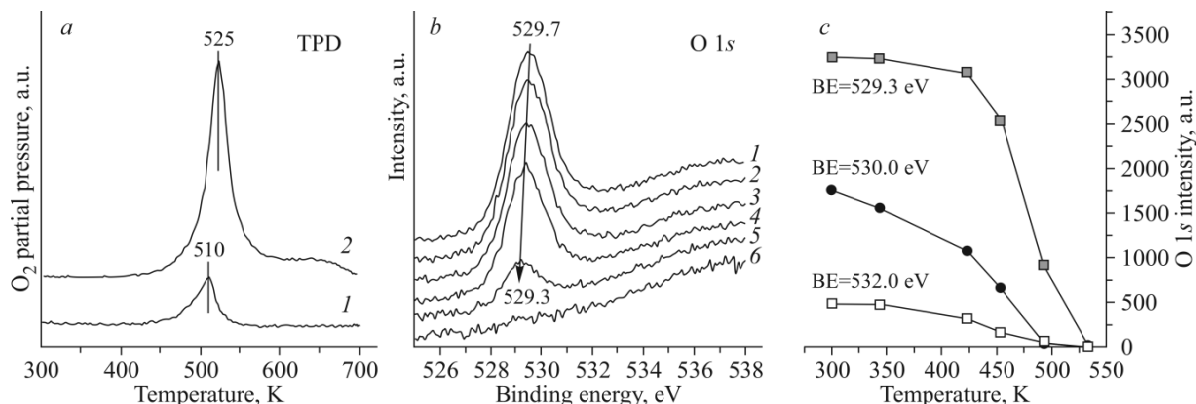


Fig. 5. TPD spectra O_2 ($m/e = 32$) of gold samples oxidized for (1) 1 min, (2) 160 min (a); O 1s spectra obtained by stepwise heating of the 2D gold oxide at (1) 300 K, (2) 344 K, (3) 423 K, (4) 453 K, (5) 493 K, (6) 533 K (b); decreasing intensity of the peaks of individual oxygen species in the O 1s spectrum upon stepwise heating (c).

speed [65]. This confirms the fact that the action of atomic oxygen on the gold surface first leads to the formation of an adsorbed oxygen layer and then to the 2D gold oxide phase.

In the TPD spectra of the maximally oxidized surface with a fully formed 2D oxide layer, the maximum of the oxygen desorption peak shifts towards higher temperatures up to 525 K (Fig. 5a, 2). The observed TPD peak has a small width (~ 10 K) characteristic for phase degradation [65].

The O 1s spectra obtained by stepwise heating showed complete desorption of oxygen at 493–533 K (Fig. 5b), in agreement with the above TPD data. The analysis of decomposed O 1s spectra (Fig. 5c) revealed that the oxygen α_2 -state was the first one to disappear ($E_b(O\ 1s) = 530.0$ eV). Thus, oxygen species are desorbed from the surface upon heating in the reverse order with respect to adsorption, thus indicating their relative transition.

The reactivity of obtained oxygen forms towards CO was studied by exposing the oxidized surface to the action of CO. The effect of CO at 298 K notably changed in the O 1s spectra (Fig. 6a) to indicate high reactivity of obtained oxygen species. Decomposition of O 1s spectra into individual components revealed that the α_1 -O peak intensity decreased as a result of CO treatment (Fig. 6b). The amount of other oxygen forms is not decreased during the interaction with CO or is decreased

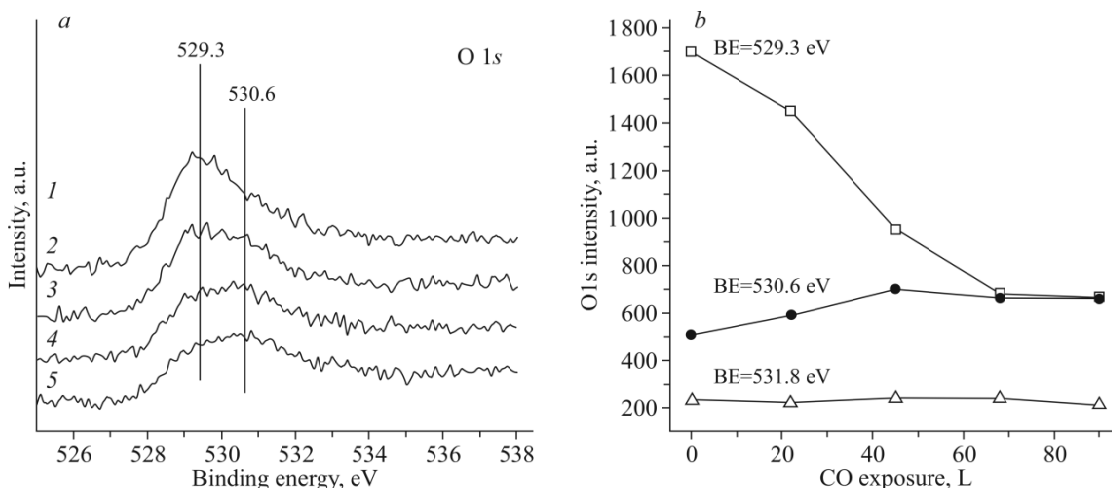


Fig. 6. O 1s XPS spectra of the gold surface oxidized for 10 min and then exposed to CO at 298 K under $P_{CO} = 1 \cdot 10^{-7}$ mbar. CO treatment: (1) 0 L, (2) 20 L, (3) 45 L, (4) 70 L, (5) 90 L (a); intensity of individual oxygen components in the composition of the O 1s peak depending on the dose of CO exposure (b).

with slight intensity changes, possibly due to structural changes on the surface. Reactivity of the species of α_1 -O atomic oxygen adsorbed on the gold surface is estimated to be quite high ($\chi \approx 0.01$) and exceeds the probability of reactivity of other species. Note that the transformation of the adsorption layer (α_1 -O species) into the surface oxide O_{so} (α_1 -O and α_2 -O species) was accompanied by a 1.5-2 fold reactivity decrease, indicating that the gold surface undergoes structural rearrangement during the surface oxide formation.

Particular interest in gold catalysts is related to their ability to perform selective CO oxidation in excess hydrogen or partial oxidation of hydrocarbons [3, 15-17]. Therefore, we compared the reactivity of the 2D gold oxide O_{so} in the oxidation reaction of various gases under equal conditions. Samples with a similar oxygen coating were exposed to pure CO, C_2H_4 , and H_2 at 373 K and under a pressure of $4 \cdot 10^{-7}$ mbar. The results of the XPS spectrokinetic studies are shown in Fig. 7. Maximum and minimum rates of the decrease of oxygen content on the gold surface were observed for the interaction with CO and hydrogen, respectively. In the case of hydrogen-oxygen titration at room temperature, the time required to remove oxygen from the surface increases by almost an order of magnitude. Calculated reactivities for different gases are shown in the inset to Fig. 7. The reactivity of the 2D gold oxide in hydrogen oxidation is 250 times lower than that in CO oxidation.

The conducted experiments show that initial stages of gold surface oxidation by a flow of atomic oxygen lead to the formation of the α_1 oxygen state with $E_b(O 1s) = 529.3$ eV (~ 0.1 - 0.5 ML thick oxygen coating). This stage of adsorption is not accompanied by the cleavage of Au-Au bonds or by oxygen diffusion into the subsurface region. The Au 4f spectra slightly changed: the electron density decreased at 83.6 eV (surface gold atoms) and increased at 84.5 eV, indicating that the interaction with oxygen creates positive charge on the gold atoms of the surface layer. The oxygen coating grows with increasing duration of exposure to atomic oxygen. After the coating thickness reaches 0.6- 0.8 ML, the second stage of oxidation of the upper gold layer begins; at this stage, the oxidized state with $E_b(Au 4f) = 85.5$ eV appears when oxygen penetrates between the first and second layers of gold atoms. This oxygen corresponds to the α_2 state characterized by $E_b(O 1s) = 530.0$ eV in the XPS spectra. Since the α_1 and α_2 states of oxygen have close binding energies, they are often not resolved in XPS spectra. In our experiments, the second state of oxygen in the subsurface layer manifested as a shift of the O 1s line towards higher binding energies from 529.3 eV to 529.6 eV. Formation of the 2D gold oxide α_{so} ($\alpha_{so} = \alpha_1 + \alpha_2$) is completed after 60-180 min of treatment, and no further surface oxidation does not occur. The amounts of oxygen on the surface (α_1) and in the subsurface region (α_2) are comparable and provide the total oxygen coating of the second monolayer.

The obtained XPS data reliably show that the 2D gold oxide consists of one layer of gold atoms and two layers of oxygen atoms located above and below the gold (Fig. 8). The stoichiometry of the 2D oxide obtained from the XPS experiments gives a ratio close to Au:O = 1.8. It is smaller than the value that was theoretically derived for AuO_2 in [66]. In this work, Sun et al. showed that the most energetically favorable structures on the gold surface (in particular, Au(111) faces)

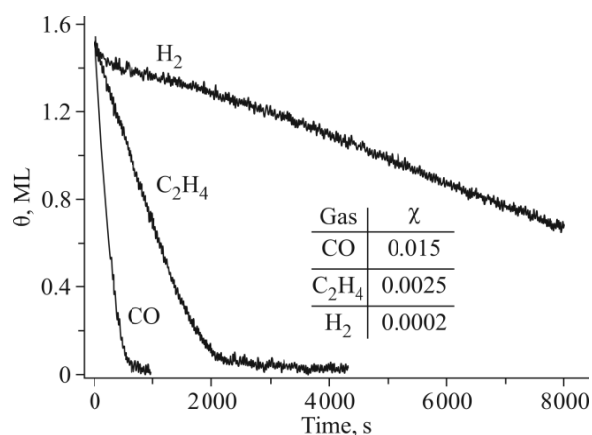


Fig. 7. Integral amount of oxygen on the gold surface depending on the time of gas exposure at 373 K under $P = 4 \cdot 10^{-7}$ mbar.

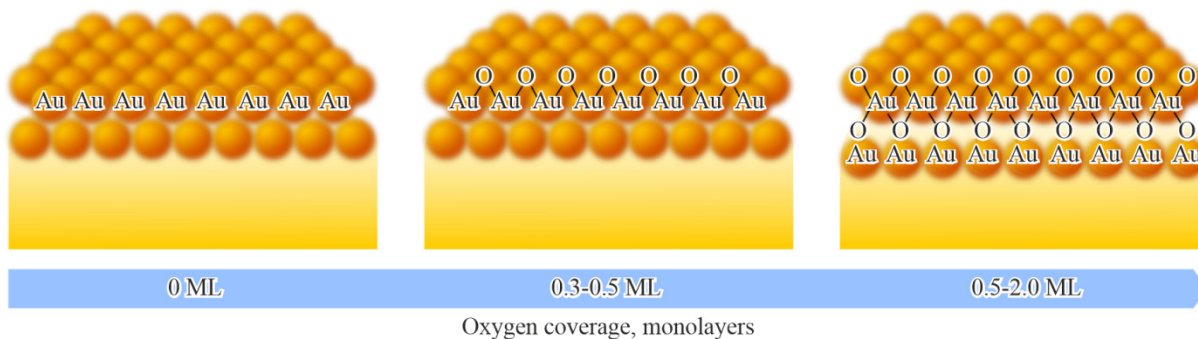


Fig. 8. Schematic formation of the AuO₂ surface oxide.

are chained single and double structures containing [AuO₄] as the primary fragment. The oxide layer thickness estimated from the XPS spectra is ~3 Å. This 2D oxide is stable up to 510 K. During thermal desorption, oxygen is removed from the surface due to direct recombination of α_1 surface oxygen atoms, and the loss of oxygen is counteracted by oxygen diffusion from the subsurface region (α_2) to the surface.

A similar structure of surface oxides was proposed for other metals such as palladium [67-70] and platinum [71, 72], which fact confirms the model of surface gold oxide proposed in our work. Properties of the resulting 2D oxide may be of practical interest, since 2D gold oxide clusters are considered to be more active than 3D ones.

When studying the reactivity of the 2D gold oxide α_{so} , it was found that oxygen of this type can oxidize CO quite efficiently at room temperature. The reactivity of oxygen in the 2D oxide (χ) is equal to 0.01 and 0.015 at 298 K and 373 K, respectively. The use of other gases (ethylene and hydrogen) demonstrated high selectivity of this oxygen species towards CO oxidation. The reactivity in the oxidation of ethylene and hydrogen at 373 K is 0.0025 and 0.0001, respectively. Thus, the oxygen of the 2D oxide is 250 times more active in CO oxidation than in H₂ oxidation.

The data on gold particles reactivity can explain high selectivity of CO oxidation in excess hydrogen (PROX reaction) on nanodispersed gold catalysts. High reactivity of α_1 -O in CO oxidation and low reactivity in H₂ oxidation suggest that these oxygen species are key intermediates in the PROX reaction mechanism. To obtain α_1 -O from O₂, O₂ molecules are to be activated for their dissociation; this process can proceed easier on flat nanoscale catalysts with active participation of the support.

CONCLUSIONS

Oxygen adsorption on a the gold foil surface was studied by XPS and TPD methods. An oxygen flow in the form of a mixture of oxygen molecules and atoms was used to prepare a wide range of oxygen coatings up to two monolayers and to study all oxygen species formed on the gold surface.

It was shown that a layer of chemisorbed atomic oxygen with a maximum coating $\Theta_{max} = 0.5$ ML was formed at the initial stages of treating the polycrystalline gold surface with atomic oxygen. As the oxygen coverage increased, the adsorption layer transformed into a 3 Å thick 2D gold oxide having a stoichiometry close to AuO₂ and stable up to = 510 K. It was found that the surface oxide structure contains two nonequivalent oxygen states, one adsorbed on the surface and the other located in the subsurface layer. It was hypothesized that the 2D oxide is formed due to the penetration of adsorbed oxygen into the subsurface region and subsequent structural rearrangement.

It was shown that the 2D oxide oxygen is highly active in CO oxidation ($\chi = 10^{-2}$). It was been established that the interaction of the 2D oxide oxygen with CO is 250 times more efficient than the H₂ oxidation. The data obtained on the reactivity of adsorbed oxygen can be used to explain high activity and selectivity of gold catalysts in the predominant CO oxidation in excess hydrogen.

FUNDING

This work was funded by the Ministry of Science and Higher Education of the Russian Federation within State Assignment for the Institute of Catalysis SB RAS (project AAAA-A21-121011390053-4).

CONFLICT OF INTERESTS

The authors declare that they have no conflicts of interests.

REFERENCES

1. M. Haruta. Gold catalysts prepared by coprecipitation for low-temperature oxidation of hydrogen and of carbon monoxide. *J. Catal.*, **1989**, *115*(2), 301-309. [https://doi.org/10.1016/0021-9517\(89\)90034-1](https://doi.org/10.1016/0021-9517(89)90034-1)
2. M. Haruta, S. Tsubota, T. Kobayashi, H. Kageyama, M. J. Genet, and B. Delmon. Low-temperature oxidation of CO over gold supported on TiO₂, α -Fe₂O₃, and Co₃O₄. *J. Catal.*, **1993**, *144*(1), 175-192. <https://doi.org/10.1006/jcat.1993.1322>
3. M. Haruta and M. Daté. Advances in the catalysis of Au nanoparticles. *Appl. Catal., A*, **2001**, *222*(1/2), 427-437. [https://doi.org/10.1016/s0926-860x\(01\)00847-x](https://doi.org/10.1016/s0926-860x(01)00847-x)
4. G. C. Bond and D. T. Thompson. Catalysis by gold. *Catal. Rev.*, **1999**, *41*(3/4), 319-388. <https://doi.org/10.1081/cr-100101171>
5. F. Boccuzzi, A. Chiorino, M. Manzoli, D. Andreeva, T. Tabakova, L. Ilieva, and V. Iadakov. Gold, silver and copper catalysts supported on TiO₂ for pure hydrogen production. *Catal. Today*, **2002**, *75*(1-4), 169-175. [https://doi.org/10.1016/s0920-5861\(02\)00060-3](https://doi.org/10.1016/s0920-5861(02)00060-3)
6. M. A. P. Dekkers, M. J. Lippits, and B. E. Nieuwenhuys. CO adsorption and oxidation on Au/TiO₂. *Catal. Lett.*, **1998**, *56*, 195-197. <https://doi.org/10.1023/A:1019037902776>
7. R. Meyer, C. Lemire, S. K. Shaikhutdinov, and H.-J. Freund. Surface chemistry of catalysis by gold. *Gold Bull.*, **2004**, *37*(1/2), 72-124. <https://doi.org/10.1007/bf03215519>
8. A. S. K. Hashmi and G. J. Hutchings. Gold catalysis. *Angew. Chem., Int. Ed.*, **2006**, *45*(47), 7896-7936. <https://doi.org/10.1002/anie.200602454>
9. T. A. Baker, X. Liu, and C. M. Friend. The mystery of gold's chemical activity: local bonding, morphology and reactivity of atomic oxygen. *Phys. Chem. Chem. Phys.*, **2011**, *13*(1), 34-46. <https://doi.org/10.1039/c0cp01514h>
10. P. Rodriguez and M. T. M. Koper. Electrocatalysis on gold. *Phys. Chem. Chem. Phys.*, **2014**, *16*(27), 13583-13594. <https://doi.org/10.1039/c4cp00394b>
11. J. Gong. Structure and surface chemistry of gold-based model catalysts. *Chem. Rev.*, **2012**, *112*(5), 2987-3054. <https://doi.org/10.1021/cr200041p>
12. L. B. Vilhelmsen and B. Hammer. Identification of the catalytic site at the interface perimeter of Au clusters on rutile TiO₂ (110). *ACS Catal.*, **2014**, *4*(6), 1626-1631. <https://doi.org/10.1021/cs500202f>
13. H. Lian, M. Jia, W. Pan, Y. Li, W. Zhang, and D. Jiang. Gold-base catalysts supported on carbonate for low-temperature CO oxidation. *Catal. Commun.*, **2005**, *6*(1), 47-51. <https://doi.org/10.1016/j.catcom.2004.10.012>
14. F. Somodi, I. Borbáth, M. Hegedűs, K. Lázár, I. E. Sajó, O. Geszti, S. Rojas, J. L. G. Fierro, and J. L. Margitfalvi. Promoting effect of tin oxides on alumina-supported gold catalysts used in CO oxidation. *Appl. Surf. Sci.*, **2009**, *256*(3), 726-736. <https://doi.org/10.1016/j.apsusc.2009.08.049>
15. O. H. Laguna, F. Romero Sarria, M. A. Centeno, and J. A. Odriozola. Gold supported on metal-doped ceria catalysts (M = Zr, Zn and Fe) for the preferential oxidation of CO (PROX). *J. Catal.*, **2010**, *276*(2), 360-370. <https://doi.org/10.1016/j.jcat.2010.09.027>

16. L. Ilieva, G. Pantaleo, I. Ivanov, R. Zanella, J. W. Sobczak, W. Lisowski, A. M. Venezia, and D. Andreeva. Preferential oxidation of CO in H₂ rich stream (PROX) over gold catalysts supported on doped ceria: Effect of water and CO₂. *Catal. Today*, **2011**, 175(1), 411-419. <https://doi.org/10.1016/j.cattod.2011.05.041>
17. O. H. Laguna, M. A. Centeno, G. Arzamendi, L. M. Gandía, F. Romero-Sarria, and J. A. Odriozola. Iron-modified ceria and Au/ceria catalysts for total and preferential oxidation of CO (TOX and PROX). *Catal. Today*, **2010**, 157(1-4), 155-159. <https://doi.org/10.1016/j.cattod.2010.04.011>
18. Y. Ryabenkova, Q. He, P. J. Miedziak, N. F. Dummer, S. H. Taylor, A. F. Carley, D. J. Morgan, N. Dimitratos, D. J. Willock, D. Bethell, D. W. Knight, D. Chadwick, C. J. Kiely, and G. J. Hutchings. The selective oxidation of 1,2-propanediol to lactic acid using mild conditions and gold-based nanoparticulate catalysts. *Catal. Today*, **2013**, 203, 139-145. <https://doi.org/10.1016/j.cattod.2012.05.037>
19. G. L. Brett, P. J. Miedziak, N. Dimitratos, J. A. Lopez-Sanchez, N. F. Dummer, R. Tiruvalam, C. J. Kiely, D. W. Knight, S. H. Taylor, D. J. Morgan, A. F. Carley, and G. J. Hutchings. Oxidative esterification of 1,2-propanediol using gold and gold-palladium supported nanoparticles. *Catal. Sci. Technol.*, **2012**, 2(1), 97-104. <https://doi.org/10.1039/c1cy00254f>
20. T. Hayashi, K. Tanaka, and M. Haruta. Selective vapor-phase epoxidation of propylene over Au/TiO₂ catalysts in the presence of oxygen and hydrogen. *J. Catal.*, **1998**, 178(2), 566-575. <https://doi.org/10.1006/jcat.1998.2157>
21. M. Turner, O. P. H. Vaughan, and R. M. Lambert. Partial oxidations with NO₂ catalyzed by large gold particles. *Chem. Commun.*, **2008**, (20), 2316. <https://doi.org/10.1039/b803828g>
22. G. Ertl. Reactions at surfaces: from atoms to complexity (Nobel lecture). *Angew. Chem., Int. Ed.*, **2008**, 47(19), 3524-3535. <https://doi.org/10.1002/anie.200800480>
23. G. A. Somorjai and J. Y. Park. Molecular surface chemistry by metal single crystals and nanoparticles from vacuum to high pressure. *Chem. Soc. Rev.*, **2008**, 37(10), 2155. <https://doi.org/10.1039/b719148k>
24. H.-J. Freund and G. Pacchioni. Oxide ultra-thin films on metals: new materials for the design of supported metal catalysts. *Chem. Soc. Rev.*, **2008**, 37(10), 2224. <https://doi.org/10.1039/b718768h>
25. G. C. Bond. The catalytic properties of gold. *Gold Bull.*, **1972**, 5(1), 11-13. <https://doi.org/10.1007/bf03215149>
26. P. Fuchs. Low-pressure plasma cleaning of Au and PtIr noble metal surfaces. *Appl. Surf. Sci.*, **2009**, 256(5), 1382-1390. <https://doi.org/10.1016/j.apsusc.2009.08.093>
27. B. Koslowski, H.-G. Boyen, C. Wilderotter, G. Kästle, P. Ziemann, R. Wahrenberg, and P. Oelhafen. Oxidation of preferentially (111)-oriented Au films in an oxygen plasma investigated by scanning tunneling microscopy and photoelectron spectroscopy. *Surf. Sci.*, **2001**, 475(1-3), 1-10. [https://doi.org/10.1016/s0039-6028\(00\)00986-9](https://doi.org/10.1016/s0039-6028(00)00986-9)
28. A. I. Stadnichenko, S. V. Koshcheev, and A. I. Boronin. Oxidation of the polycrystalline gold foil surface and XPS study of oxygen states in oxide layers. *Moscow Univ. Chem. Bull.*, **2007**, 62(6), 343-349. <https://doi.org/10.3103/s0027131407060090>
29. J. M. Gottfried, K. J. Schmidt, S. L. M. Schroeder, and K. Christmann. Spontaneous and electron-induced adsorption of oxygen on Au(110)-(1×2). *Surf. Sci.*, **2002**, 511(1-3), 65-82. [https://doi.org/10.1016/s0039-6028\(02\)01555-8](https://doi.org/10.1016/s0039-6028(02)01555-8)
30. J. M. Gottfried, K. J. Schmidt, S. L. M. Schroeder, and K. Christmann. Oxygen chemisorption on Au-(1×2) II. Spectroscopic and reactive thermal desorption measurements. *Surf. Sci.*, **2003**, 525(1-3), 197-206. [https://doi.org/10.1016/s0039-6028\(02\)02559-1](https://doi.org/10.1016/s0039-6028(02)02559-1)
31. N. B. Bazhutin, G. K. Boreskov, and V. I. Savchenko. Adsorption of molecular and atomic oxygen on gold. *React. Kinet. Catal. Lett.*, **1979**, 10(4), 337-340. <https://doi.org/10.1007/bf02075320>
32. N. D. S. Canning, D. Outka, and R. J. Madix. The adsorption of oxygen on gold. *Surf. Sci.*, **1984**, 141(1), 240-254. [https://doi.org/10.1016/0039-6028\(84\)90209-7](https://doi.org/10.1016/0039-6028(84)90209-7)
33. D. C. Lim, R. Dietsche, G. Ganteför, and Y. D. Kim. Oxidation of deposited Au_n (n = 2–13) on SiO₂/Si: Influence of the NaOH(aq) treatment. *Chem. Phys.*, **2009**, 359(1-3), 161-165. <https://doi.org/10.1016/j.chemphys.2009.03.023>
34. C. Linsmeier and J. Wanner. Reactions of oxygen atoms and molecules with Au, Be, and W surfaces. *Surf. Sci.*, **2000**, 454-456, 305-309. [https://doi.org/10.1016/s0039-6028\(00\)00215-6](https://doi.org/10.1016/s0039-6028(00)00215-6)

35. T. A. Baker, B. Xu, X. Liu, E. Kaxiras, and C. M. Friend. Nature of oxidation of the Au(111) surface: experimental and theoretical investigation. *J. Phys. Chem. C*, **2009**, 113(38), 16561-16564. <https://doi.org/10.1021/jp9052192>
36. M. M. Biener, J. Biener, and C. M. Friend. Enhanced transient reactivity of an O-sputtered Au(111) surface. *Surf. Sci.*, **2005**, 590(2/3), L259-L265. <https://doi.org/10.1016/j.susc.2005.06.003>
37. N. Saliba, D. H. Parker, and B. E. Koel. Adsorption of oxygen on Au(111) by exposure to ozone. *Surf. Sci.*, **1998**, 410(2/3), 270-282. [https://doi.org/10.1016/s0039-6028\(98\)00309-4](https://doi.org/10.1016/s0039-6028(98)00309-4)
38. J. Kim, E. Samano, and B. E. Koel. Oxygen adsorption and oxidation reactions on Au(211) surfaces: Exposures using O₂ at high pressures and ozone (O₃) in UHV. *Surf. Sci.*, **2006**, 600(19), 4622-4632. <https://doi.org/10.1016/j.susc.2006.07.057>
39. A. Y. Klyushin, T. C. R. Rocha, M. Hävecker, A. Knop-Gericke, and R. Schlögl. A near ambient pressure XPS study of Au oxidation. *Phys. Chem. Chem. Phys.*, **2014**, 16(17), 7881. <https://doi.org/10.1039/c4cp00308j>
40. I. Nakamura, A. Takahashi, and T. Fujitani. Selective dissociation of O₃ and adsorption of CO on various Au single crystal surfaces. *Catal. Lett.*, **2009**, 129(3/4), 400-403. <https://doi.org/10.1007/s10562-009-9846-9>
41. V. Dolique, A.-L. Thomann, E. Millon, A. Petit, and P. Brault. About the key factors driving the resistivity of AuO_x thin films grown by reactive magnetron sputtering. *Appl. Surf. Sci.*, **2014**, 295, 194-197. <https://doi.org/10.1016/j.apsusc.2014.01.026>
42. V. Matolín, M. Cabala, I. Matolínová, M. Škoda, J. Libra, M. Václavů, K. C. Prince, T. Skála, H. Yoshikawa, Y. Yamashita, S. Ueda, and K. Kobayashi. Au⁺ and Au³⁺ ions in CeO₂ rf-sputtered thin films. *J. Phys. D: Appl. Phys.*, **2009**, 42(11), 115301. <https://doi.org/10.1088/0022-3727/42/11/115301>
43. E. Irissou, M.-C. Denis, M. Chaker, and D. Guay. Gold oxide thin film grown by pulsed laser deposition in an O₂ atmosphere. *Thin Solid Films*, **2005**, 472(1/2), 49-57. <https://doi.org/10.1016/j.tsf.2004.06.092>
44. K. Juodkazis. XPS studies on the gold oxide surface layer formation. *Electrochem. Commun.*, **2000**, 2(7), 503-507. [https://doi.org/10.1016/s1388-2481\(00\)00069-2](https://doi.org/10.1016/s1388-2481(00)00069-2)
45. F. J. Rodríguez Nieto, E. Fachini, C. R. Cabrera, and A. J. Arvia. X-ray photoelectron spectroscopy of oxygen-containing layers formed by a linear potential scan on stepped gold (111) films in aqueous 1 M sulphuric acid. *Thin Solid Films*, **2009**, 517(5), 1534-1540. <https://doi.org/10.1016/j.tsf.2008.09.036>
46. A. M. Visco, F. Neri, G. Neri, A. Donato, C. Milone, and S. Galvagno. X-ray photoelectron spectroscopy of Au/Fe₂O₃ catalysts. *Phys. Chem. Chem. Phys.*, **1999**, 1(11), 2869-2873. <https://doi.org/10.1039/a900838a>
47. A. K. Tripathi, V. S. Kamble, and N. M. Gupta. Microcalorimetry, adsorption, and reaction studies of CO, O₂, and CO+O₂ over Au/Fe₂O₃, Fe₂O₃, and polycrystalline gold catalysts. *J. Catal.*, **1999**, 187(2), 332-342. <https://doi.org/10.1006/jcat.1999.2618>
48. T. Bär, T. Visart de Bocarmé, B. E. Nieuwenhuys, and N. Kruse. CO oxidation on gold surfaces studied on the atomic scale. *Catal. Lett.*, **2001**, 74, 127-131. <https://doi.org/10.1023/A:1016685130974>
49. A. I. Stadnichenko, E. M. Slavinskaya, E. A. Fedorova, D. A. Goncharova, V. I. Zaikovskii, T. Y. Kardash, V. A. Svetlichnyi, and A. I. Boronin. Activation of Au-CeO₂ composites prepared by pulsed laser ablation in the reaction of low-temperature CO oxidation. *J. Struct. Chem.*, **2021**, 62(12), 1918-1934. <https://doi.org/10.1134/s0022476621120118>
50. B. K. Min and C. M. Friend. Heterogeneous gold-based catalysis for green chemistry: low-temperature CO oxidation and propene oxidation. *Chem. Rev.*, **2007**, 107(6), 2709-2724. <https://doi.org/10.1021/cr050954d>
51. S. Minicò, S. Scirè, C. Crisafulli, A. M. Visco, and S. Galvagno. FT-IR study of Au/Fe₂O₃ catalysts for CO oxidation at low temperature. *Catal. Lett.*, **1997**, 47, 273-276. <https://doi.org/10.1023/A:1019081727173>
52. L. S. Kibis, A. I. Stadnichenko, E. M. Pajetnov, S. V. Koscheev, V. I. Zaykovskii, and A. I. Boronin. The investigation of oxidized silver nanoparticles prepared by thermal evaporation and radio-frequency sputtering of metallic silver under oxygen. *Appl. Surf. Sci.*, **2010**, 257(2), 404-413. <https://doi.org/10.1016/j.apsusc.2010.07.002>
53. D. A. Svintsitskiy, A. I. Stadnichenko, D. V. Demidov, S. V. Koscheev, and A. I. Boronin. Investigation of oxygen states and reactivities on a nanostructured cupric oxide surface. *Appl. Surf. Sci.*, **2011**, 257(20), 8542-8549. <https://doi.org/10.1016/j.apsusc.2011.05.012>

54. R. V. Gulyaev, A. I. Stadnichenko, E. M. Slavinskaya, A. S. Ivanova, S. V. Koscheev, and A. I. Boronin. In situ preparation and investigation of Pd/CeO₂ catalysts for the low-temperature oxidation of CO. *Appl. Catal., A*, **2012**, *439/440*, 41-50. <https://doi.org/10.1016/j.apcata.2012.06.045>
55. L. S. Kibis, A. I. Stadnichenko, S. V. Koscheev, V. I. Zaikovskii, and A. I. Boronin. Highly oxidized palladium nanoparticles comprising Pd⁴⁺ species: spectroscopic and structural aspects, thermal stability, and reactivity. *J. Phys. Chem. C*, **2012**, *116*(36), 19342-19348. <https://doi.org/10.1021/jp305166k>
56. M. H. Matloob and M. W. Roberts. Electron spectroscopic study of nitric oxide adsorbed on copper. *Phys. Scr.*, **1977**, *16*(5/6), 420-424. <https://doi.org/10.1088/0031-8949/16/5-6/040>
57. Practical Surface Analysis: by Auger and X-Ray Photoelectron Spectroscopy / Eds. D. Briggs and M. Seah. Chichester, England: Wiley, **1983**.
58. M. P. Seah and W. A. Dench. Quantitative electron spectroscopy of surfaces: A standard data base for electron inelastic mean free paths in solids. *Surf. Interface Anal.*, **1979**, *1*(1), 2-11. <https://doi.org/10.1002/sia.740010103>
59. J. F. Moulder, W. F. Stickle, P. E. Sobol, K. D. Bomben, J. Chastain, and R. C. King Jr. Handbook of X-Ray Photoelectron Spectroscopy: A Reference Book of Standard Spectra for Identification and Interpretation of XPS Data. Eden Prairie, Minnesota, USA: Perkin-Elmer, Physical Electronics Division, **1992**.
60. D. A. Svintsitskiy, A. P. Chupakhin, E. M. Slavinskaya, O. A. Stonkus, A. I. Stadnichenko, S. V. Koscheev, and A. I. Boronin. Study of cupric oxide nanopowders as efficient catalysts for low-temperature CO oxidation. *J. Mol. Catal. A: Chem.*, **2013**, *368/369*, 95-106. <https://doi.org/10.1016/j.molcata.2012.11.015>
61. D. E. Eastman, F. J. Himpsel, and J. F. van der Veen. Photoemission studies of surface core-level shifts and their applications. *J. Vac. Sci. Technol.*, **1982**, *20*(3), 609-616. <https://doi.org/10.1116/1.571405>
62. P. H. Citrin, G. K. Wertheim, and Y. Baer. Core-level binding energy and density of states from the surface atoms of gold. *Phys. Rev. Lett.*, **1978**, *41*(20), 1425-1428. <https://doi.org/10.1103/physrevlett.41.1425>
63. W. F. Egelhoff. Core-level binding-energy shifts at surfaces and in solids. *Surf. Sci. Rep.*, **1987**, *6*(6-8), 253-415. [https://doi.org/10.1016/0167-5729\(87\)90007-0](https://doi.org/10.1016/0167-5729(87)90007-0)
64. S. D. Senanayake, D. Stacchiola, P. Liu, C. B. Mullins, J. Hrbek, and J. A. Rodriguez. Interaction of CO with OH on Au(111): HCOO, CO₃, and HOCO as key intermediates in the water-gas shift reaction. *J. Phys. Chem. C*, **2009**, *113*(45), 19536-19544. <https://doi.org/10.1021/jp908169s>
65. P. A. Redhead. Thermal desorption of gases. *Vacuum*, **1962**, *12*(4), 203-211. [https://doi.org/10.1016/0042-207x\(62\)90978-8](https://doi.org/10.1016/0042-207x(62)90978-8)
66. K. Sun, M. Kohyama, S. Tanaka, and S. Takeda. Structures and stabilities of gold oxide films on gold surfaces in O₂ atmosphere. *Surf. Sci.*, **2014**, *628*, 41-49. <https://doi.org/10.1016/j.susc.2014.05.011>
67. W. Huang, R. Zhai, and X. Bao. Direct observation of subsurface oxygen on the defects of Pd(100). *Surf. Sci.*, **1999**, *439*(1-3), L803-L807. [https://doi.org/10.1016/s0039-6028\(99\)00820-1](https://doi.org/10.1016/s0039-6028(99)00820-1)
68. A. I. Titkov, A. N. Salanov, S. V. Koscheev, and A. I. Boronin. Mechanisms of Pd(110) surface reconstruction and oxidation: XPS, LEED and TDS study. *Surf. Sci.*, **2006**, *600*(18), 4119-4125. <https://doi.org/10.1016/j.susc.2006.01.131>
69. A. I. Titkov, A. N. Salanov, S. V. Koscheev, and A. I. Boronin. TDS and XPS study of oxygen diffusion into subsurface layers of Pd(110). *React. Kinet. Catal. Lett.*, **2005**, *86*(2), 371-379. <https://doi.org/10.1007/s11144-005-0337-8>
70. J.-W. He and P. R. Norton. Thermal desorption of oxygen from a Pd(110) surface. *Surf. Sci.*, **1988**, *204*(1/2), 26-34. [https://doi.org/10.1016/0039-6028\(88\)90265-8](https://doi.org/10.1016/0039-6028(88)90265-8)
71. J. Lauterbach, K. Asakura, and H. H. Rotermund. Subsurface oxygen on Pt(100): kinetics of the transition from chemisorbed to subsurface state and its reaction with CO, H₂ and O₂. *Surf. Sci.*, **1994**, *313*(1/2), 52-63. [https://doi.org/10.1016/0039-6028\(94\)91156-8](https://doi.org/10.1016/0039-6028(94)91156-8)
72. N. Mcmillan, T. Lele, C. Snively, and J. Lauterbach. Subsurface oxygen formation on Pt(100): experiments and modeling. *Catal. Today*, **2005**, *105*(2), 244-253. <https://doi.org/10.1016/j.cattod.2005.02.042>